

Passive variable rear-wing aerodynamics of an open-wheel racing car

Shinji Kajiwara¹ 

Received: 22 May 2017 / Accepted: 23 August 2017 / Published online: 31 August 2017
© Springer International Publishing AG 2017

Abstract A rear wing designed to improve motoring performance and enhance stability during cornering needs to generate a large downforce at a relatively low speed. If the angle of attack of the rear wing is large, then air resistance is increased during high-speed driving, and thus, fuel consumption is increased due to the large drag values. On the other hand, the performance on high-speed cornering will improve overall lap time with an increased angle of attack. To mitigate this disadvantage, we aimed to reduce the angle of attack during high-speed driving to reduce downforce and drag and thus to reduce fuel consumption. Meanwhile, during low-speed driving, for example in cornering, the angle of attack was increased and a large downforce generated to improve driving stability. In order to achieve both goals, we developed a passive-type variable rear wing. This rear wing was designed to have a three-step shape where the second step in the center was designed to swing. We first confirmed the behavior through both computer-aided engineering analysis and wind tunnel experiments, and then we constructed a full-size rear wing and measured the downforce on a student Formula SAE vehicle. The results showed that it is possible to generate a downforce of 80 N at a low speed of 30 km/h (8.3 m/s) and a downforce of 145 N at a high speed of 50 km/h (13.9 m/s).

Keywords Aerodynamics · Rear wing · CFD · Race car · Down force · Formula car

✉ Shinji Kajiwara
kajiwara@mech.kindai.ac.jp

¹ Department of Mechanical Engineering, Faculty of Science and Engineering, Kindai University, 3-4-1, Kowakae, Higashiōsaka, Osaka 577-8502, Japan

1 Introduction

Formula SAE is a collegiate design competition in which groups of students design, build, and race their own open-wheel racing cars. The performance of high-speed running vehicles and racing cars is strongly influenced by their aerodynamic characteristics [20], and aerodynamics have become an important factor in the design and performance of Formula SAE cars and of racing cars in general. For example, if drag is reduced, then efficiency in the high-speed range can be greatly improved. On the other hand, by increasing the downforce to a considerable degree, the kinetic performance of the vehicle in actions such as cornering can be improved. This downforce adds a lifting surface [5, 9, 11] to the car body and the ground effect of the car body [3, 15] by using or adding a wing [10, 26, 27]. But despite its being well-known that the downforce of a racing car increases with a properly designed front and rear wing, there is still little known about the influence in student Formula SAE cars [8]. To verify these effects, CAE analysis, wind tunnel experiments, measurements of actual vehicles, and so on may be employed.

Since changing the shape of an actual vehicle is complicated and expensive, it is difficult to perform a road test to examine the different parameters which are dependent on the state of the atmosphere and the road. On the other hand, CAE analysis [14, 22] is used as a complement to wind tunnel tests and has succeeded in estimating the aerodynamic force generated by a lifting surface [25]. The influence of the position and orientation of the underbody channel and the wing on the aerodynamic characteristics of a car body have also been clarified. Although the road-to-road aerodynamics are complicated by the existence of the wind tunnel's boundary layer [24], it can be avoided, as it does not exist on an actual road surface in wind tunnel

experiments using actual car shapes [4]. Thanks to a new multi-set level method, boundary layer meshes can be built over an immersed complex geometry that is applied in a metric tensor field using gradation [2]. This method allows the generation of an anisotropic semi-structured mesh with a smooth gradation of mesh size from a geometry immersed in an arbitrary coarse domain, while capturing and keeping the interface.

Flow comparisons between the experiments and CAE performance of large eddy simulations (LES) were performed and revealed that the flow structures were well captured [1]. Detached eddy simulation (DES) was performed at a lower Reynolds number (2×10^5) to satisfactorily predict the flow separations [7]. The influence of compressibility effects was investigated for high-lift aerodynamic designs operating in close ground proximity; the effects of compressibility are significant at speeds well below the Mach 0.3 threshold normally applied [16]. Previous studies of racing car aerodynamics have shown that small changes in parameters for a racing car can have significant effects on aerodynamic performance [10, 12]. The addition of front and rear wings to an open-wheel racing car can produce a large amount of downforce by using a lifting body [6, 13]. These studies show that to use simulations as tools to maximize performance, a racing car must be modeled properly in both the wind tunnel and in computation. Since it is difficult to completely match wind tunnel conditions or numerical boundary conditions to track conditions, tests have been performed to determine the proper way to evaluate the effects of wings on a racing car. An isolated full-size rear wing and a 40% scale model of a vintage Indy car have been compared [18]. The comparison revealed that the performance of the wing is enhanced by the presence of the car, indicating some degree of cross-coupling between the wing and the body. However, it is feasible to perform these tests separately and still be able to estimate the effects on the complete racing car.

The studies mentioned above primarily dealt with aerodynamics and the effects on the performance of an open-wheel racing car. In the case of the performance of single-element front wings with NACA 0015 [21] and 4412 airfoils [22], a comparison between experimental and computational results showed fairly good agreement at ground clearances greater than 0.1 chord lengths. The key to the research and development of aerodynamics of a racing car is to provide sufficient downforce and minimum aerodynamic drag. The rear wing is an essential part of the aerodynamic package of a racing car. However, the existence of a rear wing inevitably increases aerodynamic drag. How to balance the downforce and aerodynamic drag of rear wings has been an ongoing concern. The aerodynamic characteristics of a rear wing are affected by many parameters, such as the angle of attack, camber, and profile

of the airfoil. The aerodynamic performance of a multi-element airfoil in a rear wing was studied using numerical and experimental methods. If the rear wing's angle of attack is designed to be large, so as to generate a large downforce at low speed, then the air resistance will become large during high-speed driving, so the performance and fuel economy will decrease. In order to mitigate this disadvantage, we aim to reduce the angle of attack during high-speed driving in order to reduce downforce and drag and thus reduce fuel consumption. Meanwhile, during low-speed driving such as cornering, the angle of attack is increased and a large downforce is generated to improve driving stability. In order to make these different approaches compatible, we studied the passive variable rear wing. However, it is only with properly designed wing shape. In case of a badly designed wing shape, the flow around the wing surface will stall which will significantly reduce downforce by simultaneously increased drag. Thus, it is necessary to design the airfoil shape carefully.

2 Concept and design of passive variable rear-wing

2.1 Concept

A rear wing for an automobile is composed of a transverse board shaped like a wing of an airplane turned upside down and wing end plates attached to each end of it. With a rear wing installed on the rear part of a car body and generating a downforce to hold a moving car against the ground, the grip force of the rear tire increases, which improves cornering performance, acceleration performance, and stability at high speed. However, in proportion to the square of the speed, drag occurs in a direction opposite to the direction of travel of the running car. By adjusting the shape of the wing, a rear wing can achieve both a reduction in air resistance and an improvement in downforce.

In order to evaluate the aerodynamic performance, the lift coefficient C_L related to the downforce F_L , and the air resistance coefficient C_D related to the drag F_D were used. The smaller the C_L value is below zero, the greater the downforce, and the larger the C_D value, the greater the drag. The relationship between the lift coefficient C_L , the downforce F_L , and the air resistance coefficient C_D , and the drag F_D is expressed by the following equations:

$$F_L = \frac{1}{2} C_L \rho S v^2, \quad (1)$$

$$F_D = \frac{1}{2} C_D \rho S v^2, \quad (2)$$

where the variables and constants are as follows: F_L downforce, N; C_L lift coefficient; F_D drag force, N; C_D air

resistance coefficient; ρ air density, kg/m^3 ; S front projected area, m^2 ; v airspeed, m/s .

Since the downforce and drag are proportional to the square of the speed, it can be seen that the resistance due to air rapidly increases as the speed increases. By making C_L a large negative value, the contact between the tire and the ground improves and the road grip is enhanced. On the other hand, by reducing the air drag coefficient C_D , air resistance can be reduced and fuel consumption can be improved.

2.2 Wing profile

For the cross section of the wing, we chose the Airfoil Tools BE50 original [17, 23], which is often used for automobile rear wings, owing to its good manufacturability, light weight, and low resistance. BE50 has max thickness 7.3% at 25% chord and max camber 4.1% at 45% chord. The wing actually produced was intended to be attached upside down to a student Formula SAE vehicle, with a wing width of 1 m. Generally, the rear wing is fixed to the blade end plate, and the angle of the flap does not change during running. In this case, the values of C_L and C_D are constant, and the downforce during cornering and low-speed running can be obtained, but drag occurs during high-speed running and the acceleration performance deteriorates. Figure 1a shows the cross-sectional shape of BE50 original. Figure 1b shows a schematic diagram of the main wing. Also Fig. 1c shows a schematic view of the three-stage rear wing.

An ideal wing would have large C_L when cornering or during low-speed running, with a large downforce generated, and small C_D during high-speed running. Therefore, it is desirable to have both small C_L and C_D , by causing the rear wing to collapse or be variable, such that the angle of attack becomes small. There is drag reduction system (DRS) that reduces drag. However, because it is an electric type, advanced electronic control is necessary. To develop a passive-type rear wing, we investigate mechanical wings with a flow rate that is passively variable with speed. In the passive-type wing, a mechanism is required such that the wing rises when traveling at low speed and falls at high speed. The position of the shaft for this rotation was set near the center of gravity of the wing so as to reduce the influence of acceleration/deceleration of the vehicle and 10% tip side of chord was set so that passive operation could be performed smoothly. We designed a passive-type wing with a structure giving rotation springing and rotation damping around its rotation axis. According to the rule of the size of the wing, the chord length was determined to be 500 mm for the first-stage wing, the second stage was set to 300 mm which is 60% of the first-stage, and the third stage was set to 180 mm of 60% of the second stage.

3 CAE analysis

3.1 CAE analysis method

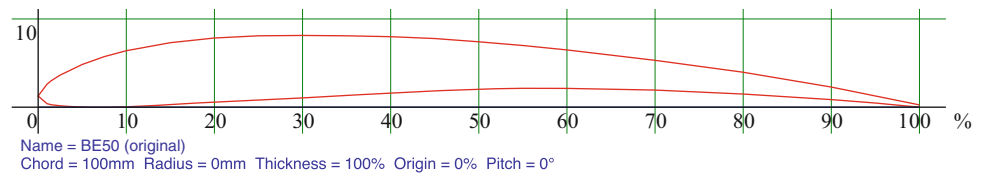
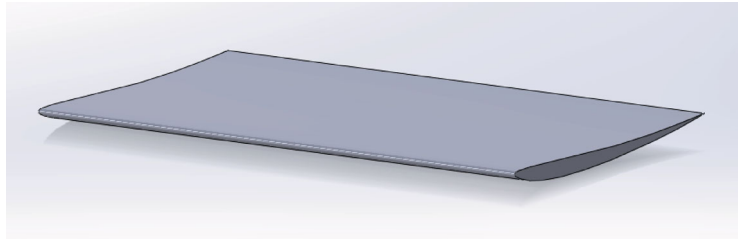
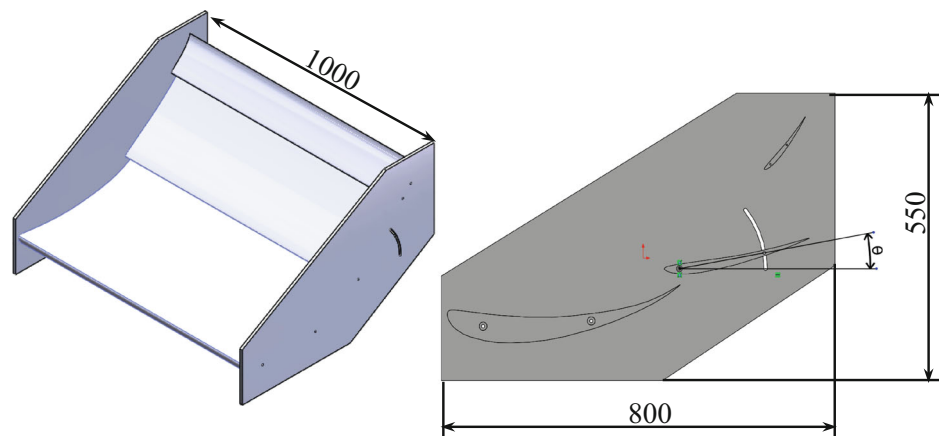
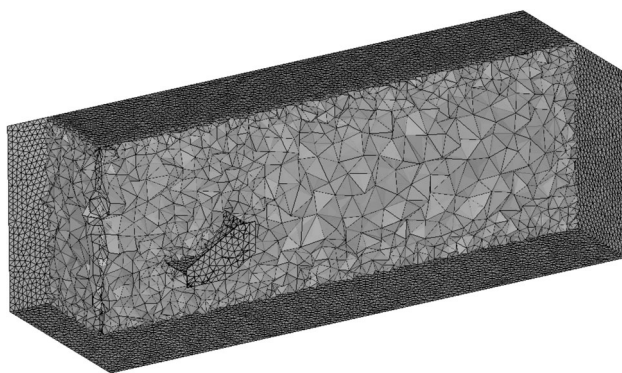
In order to produce a large downforce during low-speed traveling and to reduce drag during high-speed traveling, optimum attack angles for the rear wing during both low-speed and high-speed running are obtained through computational fluid dynamics (CFD). Originally, the synergistic effects the rear wing with the car surface is important, but this time we only analyzed the rear wing for the purpose of confirming the three-stage-rear wing effect independently. Reynolds number (Re) is 9.01×10^5 at 13.9 m/s, and 5.42×10^5 at 8.37 m/s. Here, the representative length is set to 980 mm that is the total code lengths of the three wings. In this rear wing design, Reynolds number is smaller than 1×10^6 which is the minimum of regular airfoil design. Besides, the flow is a complicated flow because of the three-stage wing. The aerodynamic characteristics of the airfoil at the low Reynolds number has a nonlinearity in the lift coefficient and at the same time the stalling characteristic also changes [19]. Therefore, it is necessary to design that the separation flow does not occur as much as possible on the lower surface of the wings.

The tool used is Cradle SCRYU/Tetra for Windows, version 12, with an Intel Xeon 3.00 GHz CPU, 4.00 GB of memory, on Windows 7 Ultimate. The calculation time was approximately 10 h. In order to improve the accuracy of separating flow analysis, boundary layer elements with thickness of 0.2 mm are inserted. The number of boundary layers is 3. Thus, the total number of points in the mesh is approximately 1,000,000. The mesh arrangement is shown in Fig. 2.

The flow is treated as a turbulent flow. The RANS equations are used to model the turbulent flow and the turbulence model is the low-Reynolds-number $k - \varepsilon$ turbulence model. The boundary condition was set at the inflow and the speed of the flow was set to range from 5.6 m/s (20 km/h) to 16.7 m/s (60 km/h). To obtain the values of C_L and C_D for a given angle of attack of each rear wing, we created 3D models of the rear wing with angles of attack ranging from 10° to 50° with increments of 10° . The 3D CAD models of the rear wing with angles of attack of 50° – 10° are shown in Fig. 3.

3.2 CAE analysis results

As an example of the analysis results, the pressure contours around the rear wing with an attack angle of 50° are shown in Fig. 4a. The streamlines around the rear wing with an attack angle of 40° are shown in Fig. 4b. From these results, it can be seen that at an attack angle of 40° , the air

Fig. 1 Schematic view of wing**(a)** Profile of BE50 (original)(UIUC Airfoil Data Site; <http://airfoiltools.com/airfoil/details?airfoil=be50-il>)**(b)** 3D image of BE50 wing**(c)** Three-stage rear wing**Fig. 2** Mesh arrangements

flows between the second and third panels of the wing and the pressure drops. Thus, it is expected that the resistance will decrease. At 50° , since all the streamlines are heading upward and it is not observed separation flow near the lower surface of the wing. It is predicted that downforce is

efficiently generated like with a single wing. In case of a bad designed series of wings the flow will stall that will significantly reduce downforce by simultaneously increased drag. Based on the analysis results, C_L achieves a maximum when the second wing angle is 50° . Figure 5a shows the relationship between vehicle speed and downforce while Fig. 5b shows the relationship between vehicle speed and drag. As can be seen from Fig. 5a, the downforce is larger at 40° than at 50° . On the other hand, drag is almost the same at 40° and at 50° from Fig. 5b.

From these CAE results and Eqs. (1) and (2), the relationship between C_D and C_L is calculated and plotted on a graph in Fig. 6. From Fig. 6, at low speed, it can be seen that the value of C_D/C_L is optimal at 40° . At high speed, C_D and C_L are the smallest at 10° , indicating this is optimal. Thus, the rear wing should be designed to be variable with an initial attack angle of 40° at a low speed of 8.3 m/s (30 km/h) and an attack angle of 10° at high speed of 13.9 m/s (50 km/h), such that C_D and C_L are the smallest.

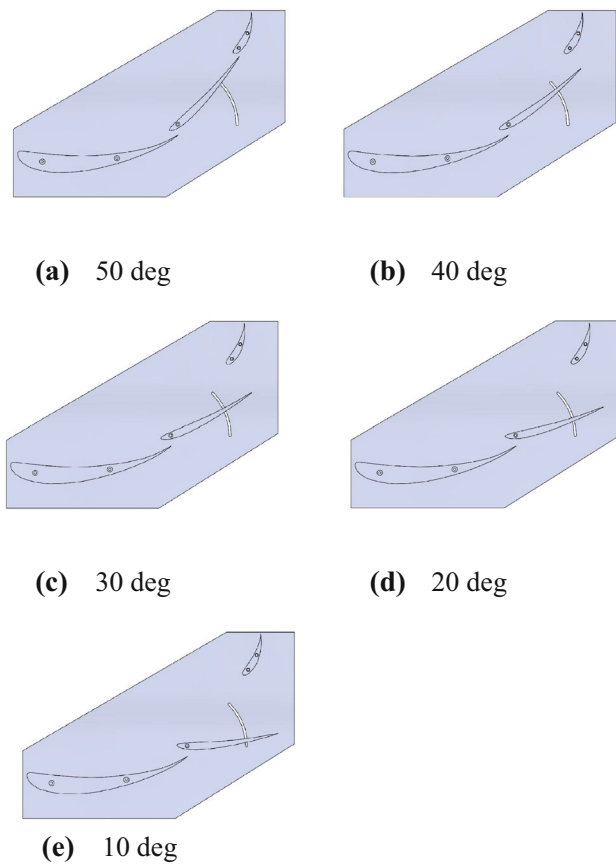


Fig. 3 3D-CAD models of the rear wing with angles of attack of 50°–10°

4 Wind tunnel experiment

In order to verify the results of the CAE analysis, we constructed a 1/8th-size scale model and tested it in a smoke-filled wind tunnel. The blade length of the scale model was 120 mm. In order to easily observe the flow in the wind tunnel experiment, the wing’s end plates were made of a transparent acrylic plate. A photo of the experimental 1:8 scale model of three-stage wing is shown in Fig. 7. The variable wing was constructed so that the angle of attack could be changed within a range of 0°–50°. We fixed the rear wing model in place using the wind tunnel’s experimental equipment and photographed it with a high-speed camera. A smoke wind tunnel experiment was conducted with a flow rate of 44.4 m/s and rear wing attack angles of 40° and 10°. These tests will compare the results of CFD analysis and the flow around the rear wing in the actual scale model. Due to the wind tunnel device, the flow velocity could not be raised any further. Reynolds number in 1/8th-size scale model is 3.60×10^5 . This number corresponds to 5.56 m/s (20 km/h) in the full-size model. Therefore, the comparison has become qualitative.

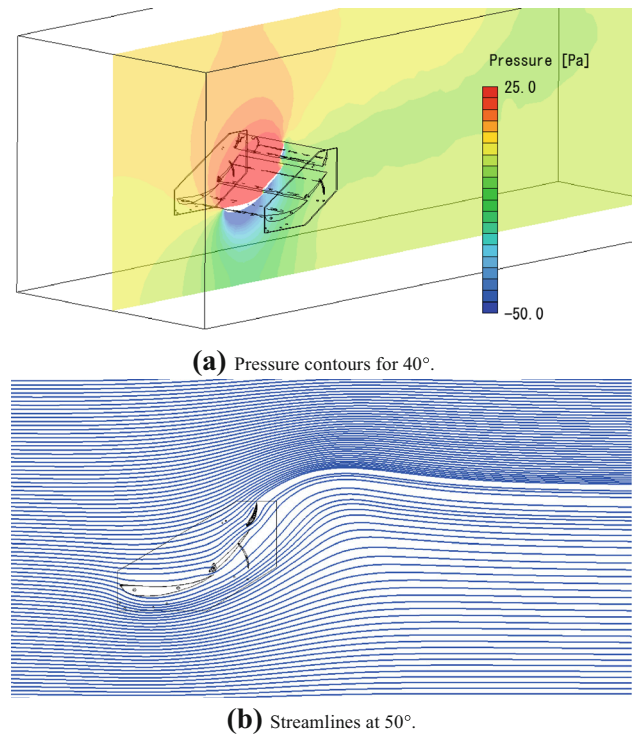


Fig. 4 Examples of CAE results

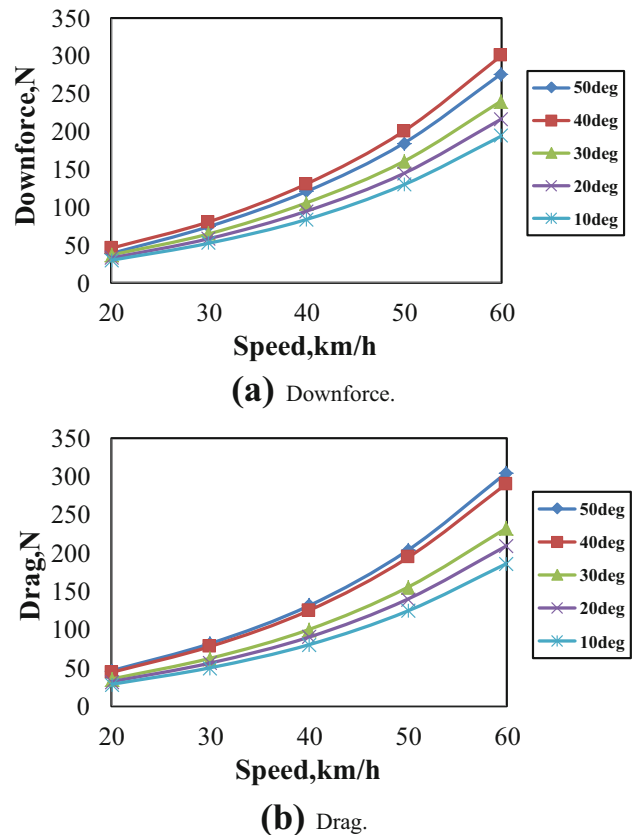


Fig. 5 Relationships between vehicle speed and downforce and drag

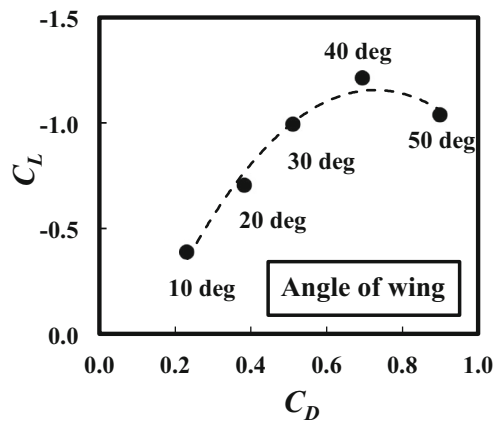


Fig. 6 Relationship between C_L and C_D for a variable rear wing

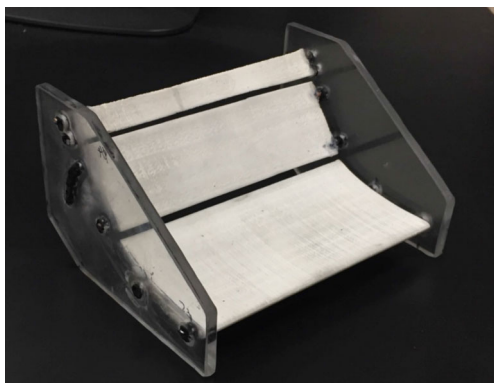


Fig. 7 Photo of the experimental 1:8 scale model of three-stage wing

However, it is sufficiently useful for observing the flow situation.

The results of the wind tunnel experiment are compared with the streamlines of the CFD analysis results in Fig. 8. Figure 8a shows the case when the angle of attack of the rear wing is 40° and Fig. 8b shows the case when the angle of attack is 10° . From Fig. 8a, the flow at the upper part of the second wing flows to the lower surface of the third wing, and it appears that downforce is effectively achieved while reducing drag. The concentration of smoke appears to be highest in the main stream. From these results, it can be seen that the wind tunnel experimental results agree well with the CAE analysis results.

5 Production and measurement of a full-size rear wing

5.1 Design and production

The full-size rear wing was designed based on the analysis results. The CAD model and a photo of the actual model are shown in Fig. 9. The wing was made of GFRP from the

production performance, and wood was used for the wing's end plates. The spring constant was set such that the portion of the second wing would undergo downforce and drag, and vary at a predetermined speed. A tension spring was attached at a position 170 mm from the rotation axis. A dynamic model of the second wing is shown in Fig. 10. The load F , resulting from the drag F_D' and downforce F_L' , applied to the tension springs in the second-stage wing is expressed by the following equation:

$$\begin{aligned} F &= F_D' \cos\left(\frac{\pi}{2} - \theta\right) + F_L' \cos \theta \\ &= F_D' \sin \theta + F_L' \cos \theta. \end{aligned} \quad (3)$$

In order to determine the strength of the spring, the moment around the shaft was obtained by CAE analysis. From the results of CAE analysis of the downforce and drag for the second-stage rear wing, the load force is calculated to be $F = 51.1$ N at a low speed of 30 km/h for a wing attack angle of 40° , and to be $F = 98.0$ N at a high speed of 50 km/h for a wing attack angle of 10° . Therefore, using Eq. (3), the spring was set to an initial tension of 50 N and a spring constant of 550 N/m.

5.2 Experimental method with an actual vehicle

Figure 11 shows how the passive rear wing is attached to the experimental vehicle. In order to actually measure downforce, a strain gauge was attached to the stay supporting the rear wing, and the force was measured. In the experiment, two sets of downforce data were measured: with a fixed wing attached and with the passive rear wing attached. Sampling was performed at 1 kHz. In addition, a DL1 data logger made by race technology was used to measure the speed and acceleration of the vehicle. A diagram of the arrangement of measuring devices is shown in Fig. 12. Measurement of the angle of attack of the passive-type rear wing was performed using a camera from the front and side directions. In actual driving, five laps were made of a course 600 m long and data were acquired.

5.3 Results of experiment

The driving experiment was performed at the closed circuit with both passive-type and fixed-type rear wing. The course map is shown in Fig. 13a. This course is 603 m in length and average lap time is around 32 s. A measured sample of GPS image of the vehicle experiment is shown in Fig. 13b. The color of each line denotes the time. Also the lap times were obtained. From the speed that is differentiated the measured time, the relationships between speed and wing attack angle and downforce were obtained. Photos of the rear wing from the front taken while driving are shown in Fig. 14. Figure 14a shows the case at 0 m/s,

Fig. 8 Results of the wind tunnel experiment and CFD analysis

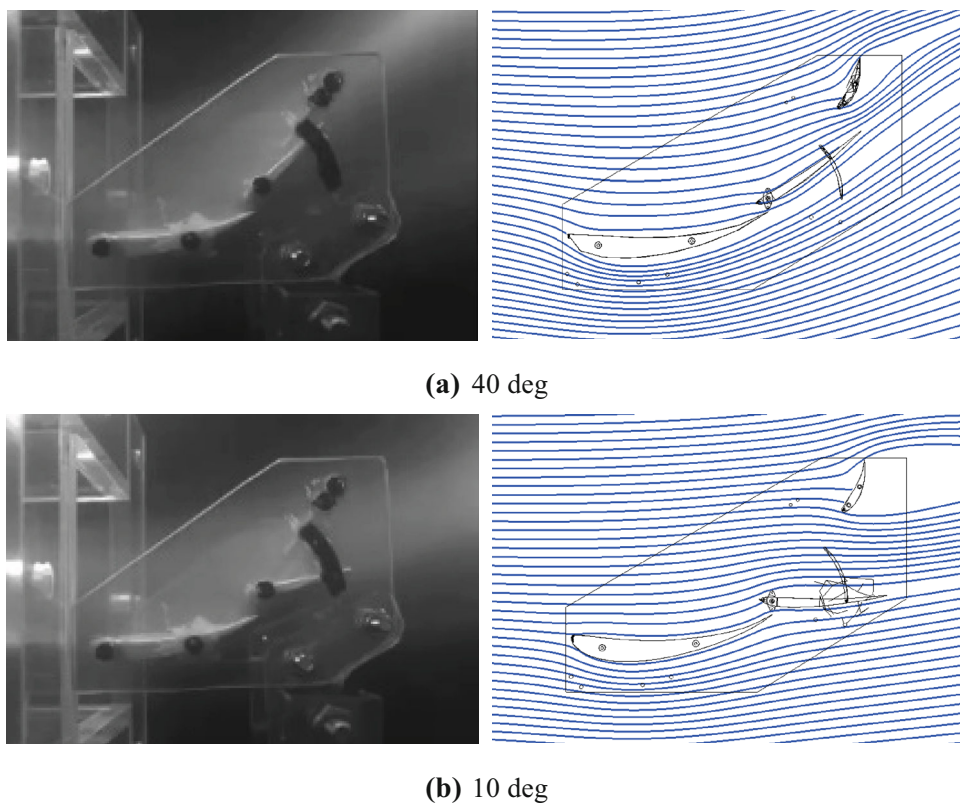


Fig. 9 CAD model and photo of the actual full-size rear wing

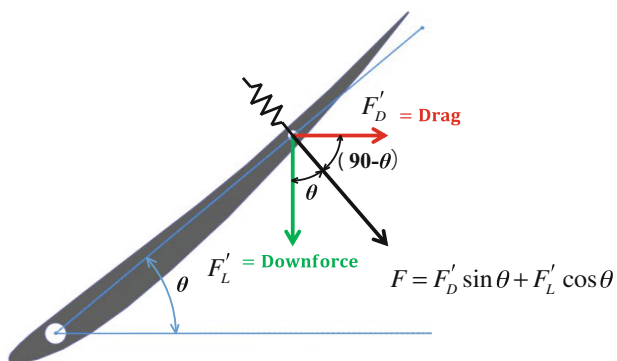
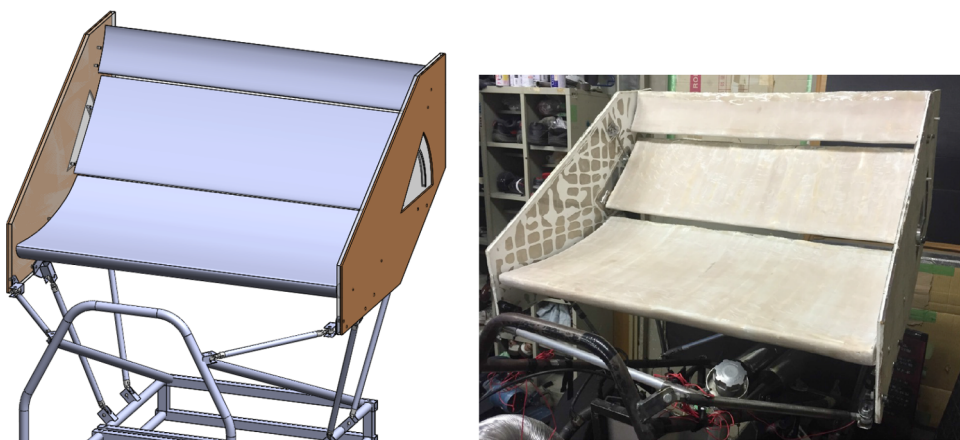


Fig. 10 Dynamic model of the second wing

Fig. 14b shows the case at 8.3 m/s (30 km/h), and Fig. 14c shows the case at 13.9 m/s (50 km/h). Side views of the passive rear wing are shown in Fig. 15. From these figures, the angle of attack was read from the side of the wing during image processing.

Figure 16 shows the measured variation in downforce over 3 s while driving at a constant speed. Figure 16a shows the case at a speed of 8.3 m/s (30 km/h) and Fig. 16b shows the case at a speed of 13.9 m/s (50 km/h). From these figures, the measured downforce at a low speed of 8.3 m/s for both the passive wing and the fixed wing are around 70–100 N. The passive wing has a slightly smaller



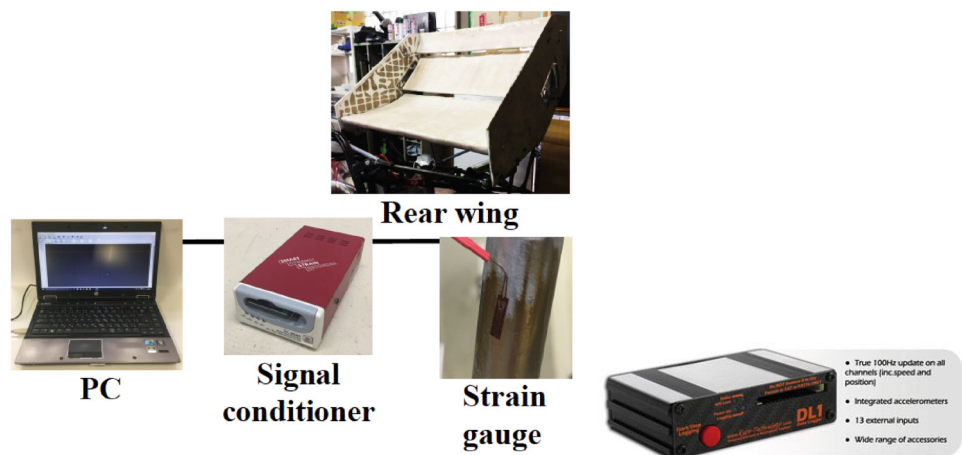
Fig. 11 Setup for driving experiment

value, owing to the influence of the vibration of the wing. On the other hand, at 13.9 m/s, the downforce of the fixed wing is approximately 175 N and for the passive wing it is approximately 150 N. Since the vibration of the wing is high, the downforce also exhibits oscillation.

Figure 17 shows the downforce measurements at 8.3 and 13.9 m/s for the passive-type variable wing and the fixed wing and the CAE analysis results. From Fig. 17, it can be seen that by changing from a fixed wing to a passive wing, the downforce at low speed can be kept the same, and at high speed it can be reduced by 14.0% from approximately 171–145 N. However, the downforce of the passive rear wing at high speed does not decrease as much as in the results of CAE analysis. This is considered to be caused by vibration resulting from the unevenness of the road surface when driving at high speed, and the corresponding change in the angle of attack.

Figure 18 shows the relationship between vehicle speed and the lift coefficient C_L . From this figure, it can be seen that at around 30 km/h, C_L exhibits little difference, but at higher speeds, the difference is greater.

Fig. 12 Diagram of the arrangement of measurement devices



(a) Downforce measurement

(b) DL1

6 Discussion

Downforce can be measured by attaching a strain gauge to the wing stay. However, since it is difficult to directly measure drag, CAE results were used for estimation. The drag was estimated from the angle of attack measured from the video recorded from the side and the speedometer using Figs. 13 and 15. At a speed of 8.3 m/s (30 km/h), the drag is estimated to be 69.4 N at an angle of attack of 40°, and at speed of 13.9 m/s (50 km/h) it was estimated to 149.2 N at an angle of attack of 10°. The estimated drags of the fixed wing and passive wing at 8.3 and 13.9 m/s are shown in Fig. 19. Figure 20 shows the relationship between vehicle speed and the drag coefficient C_D . This figure is calculated from Fig. 19 and Eq. (1). From this figure, it can be seen that C_D can be reduced. However, the downforce of the

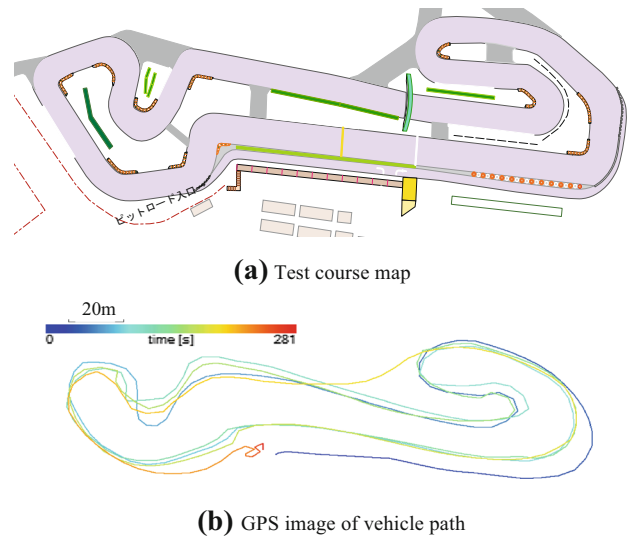


Fig. 13 Test course map and GPS image of vehicle path (600 m)

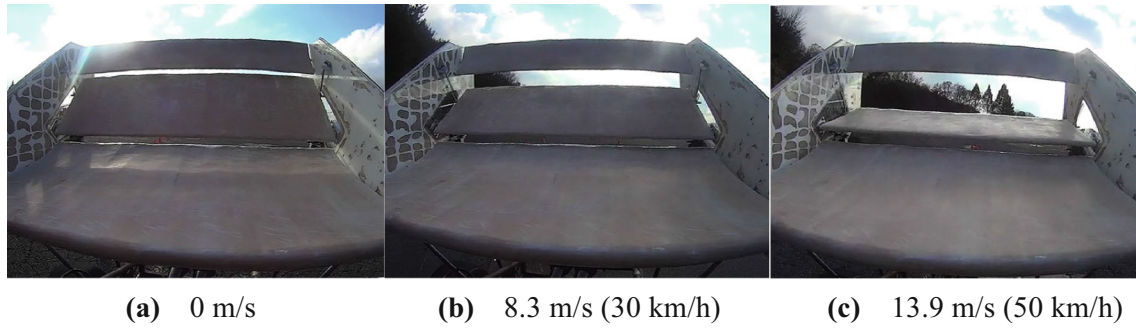


Fig. 14 Photos of the rear wing from the front



Fig. 15 Side view of the passive rear wing

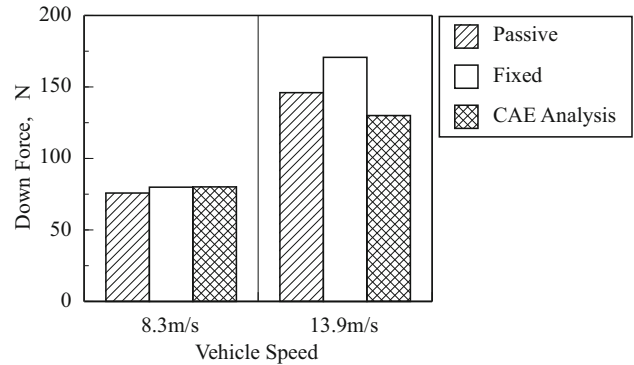
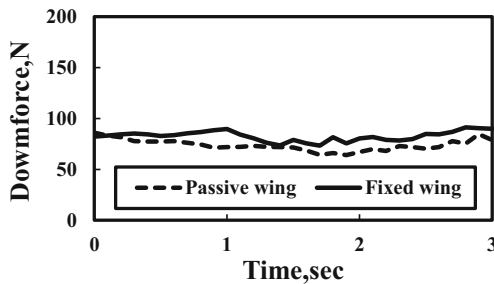
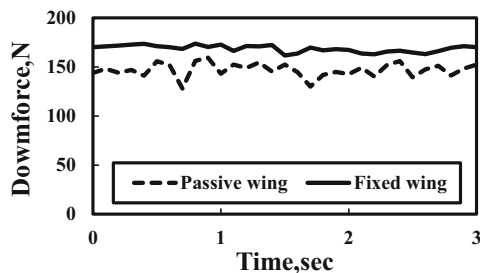


Fig. 17 Results of downforce measurements and CAE analysis



(a) 8.3 m/s (30 km/h)



(b) 13.9 m/s (50 km/h)

Fig. 16 Measured downforce

passive rear wing at high speed around 50 km/h did not decrease as much as the CAE analysis result. This is considered to be caused by the fact that the wind speed of about 2.0 m/s was blowing in the experiment, and the angle

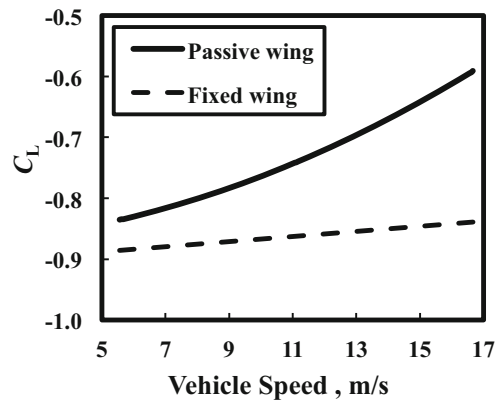


Fig. 18 Relationship between vehicle speed and lift coefficient C_L

of attack of the second-stage rear wing fluctuated due to the vibration caused by the unevenness of the road surface. From these results, it is clearly necessary to consider the implementation of a damper in the passive rear wing design in the future and to properly suppress the vibration of the wing. Furthermore, in order to optimize the lift coefficient C_L and the air resistance coefficient C_D , it is necessary to appropriately change the angle of attack depending on the vehicle speed. For that purpose, we consider it is necessary to optimize the position of the rotational axis of the wing and optimize the spring constant as a parameter in the design. From Fig. 8b, it can be seen that the third-stage

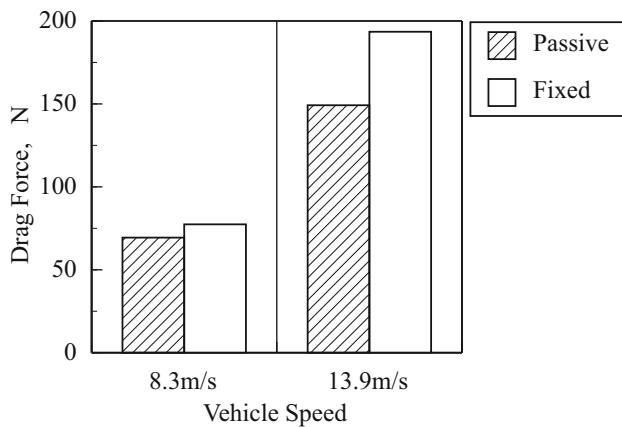


Fig. 19 Estimated drags of fixed and passive wings at 8.3 and 13.9 m/s

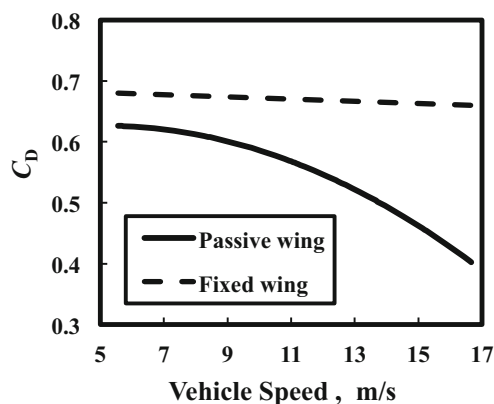


Fig. 20 Relationship between vehicle speed and estimated drag coefficient C_d

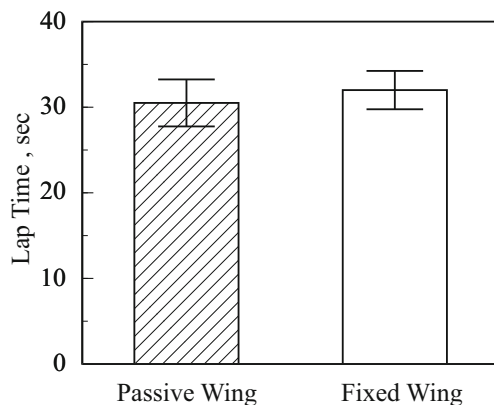


Fig. 21 Lap time comparison between passive and fixed wing

wing is stalled even at low speed. Therefore, it is considered that the performance is further improved if the third-stage wing is made variable.

As a confirmation of the effect of passive-type wing, the time was actually measured with the course shown in Fig. 13a. Lap time comparison between passive and

fixed wing is shown in Fig. 21. The average time of 30 laps was shortened to 30.5 s of the passive wing and about 1.5 s compared with 32.0 s of the normal wing. However, it was found that the passive-type wing is susceptible to the influence of the wind and the ground vibration, and the variation in the lap time becomes large.

7 Conclusion

Based on the results of CFD analysis, a passive-type variable rear wing was manufactured and measured. The passive-type rear wing generates a downforce equivalent to a fixed-type rear wing at low speed, and reduces downforce at high speed. That is, it makes it possible to reduce drag. As a confirmation of the effect of passive-type wing, the average lap time was shortened. In future, it is necessary to optimize the rotational axis and spring constant of the wing. Also, we consider it necessary to implement countermeasures against vibration from the road surface. Furthermore, if the third-stage wing can be made variable, further performance improvement can be expected.

References

- Aljure, D.E., Lehmkuhl, O., Rodríguez, I., Oliva, A.: Flow and turbulent structures around simplified car models. *Comput. Fluids* (2014). doi:[10.1186/2190-5983-4-6](https://doi.org/10.1186/2190-5983-4-6)
- Billon, L., Mesri, Y., Hachem, E.: Anisotropic boundary layer mesh generation for immersed complex geometries. *Eng. Comput.* (2017). doi:[10.1007/s00366-016-0469-7](https://doi.org/10.1007/s00366-016-0469-7)
- Burgin, K., Adey, P.C., Beatham, J.P.: Wind tunnel tests on road vehicle models using a moving belt simulation of ground effect. *J. Wind Eng. Ind. Aerodyn.* (1986). doi:[10.1016/0167-6105\(86\)90087-5](https://doi.org/10.1016/0167-6105(86)90087-5)
- Carsten, O.: Adjoint methods for car aerodynamics. *J. Math. Ind.* (2014). doi:[10.1186/2190-5983-4-6](https://doi.org/10.1186/2190-5983-4-6)
- Coiro, D.P., Nicolosi, F., Amendola, A., Barbagallo, D., Papanone, L., Beccio, S., Castelli, P., Limone, S.: Experiments and numerical investigation on a multi-component airfoil employed in a racing car wing. *SAE Pap.* (1997). doi:[10.4271/970411](https://doi.org/10.4271/970411)
- Garry, K.P.: Some effects of ground clearance and ground plane boundary layer thickness on the mean base pressure of a bluff vehicle type body. *J. Wind Eng. Ind. Aerodyn.* (1996). doi:[10.1016/S0167-6105\(96\)00054-2](https://doi.org/10.1016/S0167-6105(96)00054-2)
- Guilmineau, E., Chikhaoui, O., Deng, G., Visonneau, M.: Cross wind effects on a simplified car model by a DES approach. *Comput. Fluids* (2014). doi:[10.1016/j.compfluid.2011.08.020](https://doi.org/10.1016/j.compfluid.2011.08.020)
- Hetawala, S., Gophaneb, M., Ajay, B.K., Mulkamalak, Y.: Aerodynamic study of formula SAE car. *Proc. Eng.* (2014). doi:[10.1016/j.proeng.2014.12.398](https://doi.org/10.1016/j.proeng.2014.12.398)
- Hurst, D.W.: Modern wind tunnel testing of indycars. *SAE Pap.* (1994). doi:[10.4271/942497](https://doi.org/10.4271/942497)
- Jasinski, W., Selig, M.: Experimental study of open-wheel race-car front wings. *SAE Tech. Pap.* (1998). doi:[10.4271/983042](https://doi.org/10.4271/983042)

11. Katz, J.: Aerodynamic model for wing-generated down force on open-wheel-racing-car configurations. SAE Pap. (1986). doi:[10.4271/860218](https://doi.org/10.4271/860218)
12. Kieffer, W., Moujaesb, S., Armbyab, N.: CFD study of section characteristics of formula Mazda race car wings. Math. Comput. Model. (2006). doi:[10.1016/j.mcm.2005.03.011](https://doi.org/10.1016/j.mcm.2005.03.011)
13. Katz, J.: Investigation of negative lifting surfaces attached to an open-wheel racing car configuration. SAE Pap. (1985). doi:[10.4271/850283](https://doi.org/10.4271/850283)
14. Katz, J., Luo, H., Mestreau, E., Baum, J., Lohner, R.: Viscous-flow simulation of an open-wheel race car. SAE Publ. (1998). doi:[10.4271/983041](https://doi.org/10.4271/983041)
15. Kim, M.S., Geropp, D.: Experimental investigation of the ground effect on the flow around some two-dimensional bluff bodies with moving-belt techniques. J. Wind Eng. Ind. Aerodyn. **74–76**, 511–519 (1998) (PII:**S0167-6105(98)00046-4**)
16. Keogh, J., Doig, G., Diasinos, S.: Flow compressibility effects around an open-wheel racing car. Aeronaut. J. **118**(1210), 1409–1431 (2014)
17. Liebeck, R.H.: Design of subsonic airfoils for high lift. J. Aircr. (1978). doi:[10.2514/3.58406](https://doi.org/10.2514/3.58406)
18. Mears, A.P., Dominy, R.G., Sims-Williams, D.B.: The air flow about an exposed racing wheel. SAE Tech. Pap. (2002). doi:[10.4271/2002-01-3290](https://doi.org/10.4271/2002-01-3290)
19. Mueller, T.J.: Fixed and flapping wing aerodynamics for micro air vehicle applications. Am. Inst. Aeronaut. Astronaut. (2001). doi:[10.2514/4.866654](https://doi.org/10.2514/4.866654)
20. Pfadenhauer, M.: High-performance vehicles. In: Schuetz, T. (ed.) Aerodynamics of Road Vehicles, 5th edn. SAE International, Warrendale (2016). (ISBN **978-0-7680-7977-7**)
21. Ranzenbach, R., Barlow, J.B.: Two-dimensional airfoil in ground effect, an experimental and computational study. SAE Publ. (1994). doi:[10.4271/942509](https://doi.org/10.4271/942509)
22. Ranzenbach, R., Barlow, J.B.: Cambered airfoil in ground effect—an experimental and computational study. SAE Publ. (1996). doi:[10.4271/960909](https://doi.org/10.4271/960909)
23. Rezek, T.J., da Silva, E.R., Ramirez Camacho, R.G., Kyprianidis, K.: Multi-objective aerodynamic optimization of an unmanned aerial vehicle. Presented at the aerospace technology congress—FT2016. <http://urn.kb.se/resolve?urn=urn:nbn:se:mdh:diva-33521> (2016). Accessed 1 Feb 2017
24. Senior, A.E., Zhang, X.: The force and pressure of a diffuser—equipped bluff body in ground effect. ASME J. Fluids Eng. (2001). doi:[10.1115/1.1340637](https://doi.org/10.1115/1.1340637)
25. Sovran, G.: The kinematic and fluid-mechanic boundary conditions in underbody flow simulation. In: Proceedings of the CNR-Pininfarina Work-shop on Wind Tunnel Simulation of Ground Effect, Turin, Italy, May, published by National Research Council, 1994
26. Zerihan, J., Zhang, X.: Aerodynamics of a single element wing in ground effect. J. Aircr. **10**(2514/2), 2711 (2000)
27. Zhang, X., Zerihan, J.: Aerodynamics of a double-element wing in ground effect. AIAA J. **10**(2514/2), 2057 (2003)